FEBS Letters 569 (2004) 346–350 FEBS 28547

Calcitonin-derived carrier peptide plays a major role in the membrane localization of a peptide–cargo complex

Sylvie Boichot[a], Ulrike Krauss[b], Thomas Plénat[a], Robert Rennert[b], Pierre-Emmanuel Milhiet[a], Annette Beck-Sickinger[b], Christian Le Grimellec[a,*]

[a] *Nanostructures et Complexes Membranaires, C.B.S. CNRS UMR5048-INSERM U554, 29 rue de Navacelles, 34090 Montpellier Cedex, France*
[b] *Institute of Biochemistry, University of Leipzig, Talstr. 33, D 04103 Leipzig, Germany*

Received 3 March 2004; revised 18 May 2004; accepted 18 May 2004

Available online 15 June 2004

Edited by Gerrit van Meer

Abstract Bilayers made of dioleoylphosphatidylcholine (DOPC)/dipalmitoylphosphatidylcholine (DPPC) mixture containing or not cholesterol (Chl) were used to investigate the interaction of a carrier peptide with membranes. Atomic force microscopy revealed that the C-terminal 9-32 fragment of human calcitonin (hCT (9-32)), free or coupled to enhanced green fluorescent protein (hCT-eGFP) cargo forms aggregates in the DOPC fluid phase in absence of Chl and in the DPPC enriched liquid-ordered phase when Chl is present. The data show that hCT (9-32) plays a determinant role in the membrane localization of the peptide–cargo complex. They suggest that carpet-like mechanism for membrane destabilization may be involved in the carrier function of hCT (9-32).

Keywords: Atomic force microscopy; Cell penetrating peptide; Supported bilayer; Lipid–peptide interaction; Phosphatidylcholine; Cholesterol; Phase-separation

1. Introduction

Cell membrane carrier peptides, also called cell penetrating peptides (CPPs), deliver large hydrophilic molecules (cargo) like proteins or nucleotides to the intracellular space. The low lytic activity and high efficiency characterizing these CPPs explain they appear as promising tools in the field of drug and gene therapy [1–3]. The mechanisms involved in the peptide/cargo translocation across cells plasma membrane however remain a matter of debates. Thus, it is not clear to what extent some of the peptides require energy for cell entering [4–6]. According to the peptides, they might form carpet-like structures that destabilize the bilayer organization allowing the intracellular delivery of the cargo or induce the formation of transient pores [7–9]. How large hydrophilic cargo molecules linked to peptides affect the peptide–membrane interaction is also poorly understood.

Human calcitonin peptide C-terminal fragment 9-32 (hCT (9-32)) derived from the human calcitonin hormone (hCT) was shown to translocate cargo across cells membrane by a pathway which does not involve the hormone receptor [10,11]. Thus, hCT and hCT (9-32) were used to internalize efficiently the enhanced green fluorescent protein (eGFP) into excised nasal mucosa [12]. It is also known that hCT induces the formation of voltage-dependent channels in lipid bilayers [13]. In order to better characterize the mechanisms involved in hCT (9-32) carrier activity we have added the peptide and the peptide–eGFP complex to dioleoylphosphatidylcholine (DOPC)/dipalmitoylphosphatidylcholine (DPPC) (1:1) supported bilayers containing or not cholesterol (Chl). In this study, care was taken to add the peptide under conditions as close as possible to those for delivery of cargo into the cells. Atomic force microscopy (AFM) was used to characterize the surface topography of samples. AFM was previously shown to provide unique information on lipid–peptide interactions in both monolayers and supported bilayers [14–16].

2. Materials and methods

2.1. Materials

hCT (9-32) fragment. The peptide 9-32, fragment of human calcitonin (hCT), has the following sequence: L^{9}GTYTQDF^{16}NKFHTFP^{23}QTAIGVGAP^{32}-NH_2. It was synthesized by automated multiple solid-phase peptide synthesis (Fmoc strategy) using a robot system (Syro, MultiSynTech, Bochum, Germany) as previously described [12]. The peptide was analysed by RP HPLC and matrix assisted laser desorption ionisation (MALDI) mass spectrometry. Correct mass was found at 2610.0 (calc. 2608.3) and purity according to HPLC was >96%.

hCT (9-32)/eGFP complex. eGFP is a 239 amino acid red-shifted variant of wild-type GFP that has been optimized for brighter fluorescence and higher expression in mammalian cells. Expressed protein ligation was used to generate a construct of recombinant eGFP and the amidated hCT-derived peptide [12]. Ligation was performed by a chemical ligation strategy [17].

2.2. Methods

Preparation of supported bilayers. Supported bilayers made of DOPC/DPPC (1:1) and DOPC/DPPC/Chl (1:1:0.35) mixtures (Sigma–Aldrich, Saint Quentin-Fallavier, France) were formed from multilamellar vesicles (MLVS) as previously described [18]. The MLVs suspension (~0.3 mM) was extruded at 65 °C through 0.1 μm pore diameter polycarbonate membranes (Avanti Polar Lipids, Alabaster, AL) to obtain unilamellar vesicles. The vesicles suspension was deposited on a freshly cleaved mica surface and incubated, without exposure to air, at 65 °C for 2 h in a water bath. At the end of the incubation, the bilayers were rinsed with PBS to remove the vesicles in excess.

Atomic force microscopy. AFM observations of the bilayers were performed as previously described [15,18] on a Nanoscope IIIA (Digital Instruments, Santa Barbara, CA) equipped with a fluid cell,

* Corresponding author. Fax: +33-467- 41-79-13.
E-mail address: clg@cbs.cnrs.fr (C. Le Grimellec).

0014-5793/$22.00 © 2004 Published by Elsevier B.V. on behalf of the Federation of European Biochemical Societies.
doi:10.1016/j.febslet.2004.05.078

using a J scanner. All samples were examined under PBS (pH 7.4), in contact mode. Topographic (height) images were acquired in constant-force mode using silicon nitride tips on cantilevers with a nominal spring constant of 0.03 N/m (Park Scientific Instruments, Sunnyvale, CA), at a scan rate of 1 Hz. Typically, the scanning force was adjusted to below 0.2 nN and readjusted for drift during images acquisition. Images were obtained from at least two different samples for each condition with at least three macroscopically separated areas on each sample. Representative height images are presented.

Incubation of bilayers with hCT (9-32). Samples were first checked for the quality of the supported bilayers before addition of hCT (9-32). To avoid contamination of the AFM liquid cell by the peptide, samples were taken out of the microscope and incubated at room temperature for various times from 30 min to 18 h, according to the bilayer composition, with 150 μl of 50 μM hCT (9-32) (or hCT (9-32)/eGFP). Such a concentration is needed for hCT (9-32) acting as a carrier peptide on living cells [11,12]. At the end of the incubation period, the bilayer was rinsed with PBS at pH 7.4 and placed under the microscope.

3. Results

3.1. hCT 9-32 interaction with fluid-gel phase separated bilayers

As previously reported [18], AFM examination in buffer of DOPC/DPPC (1:1) revealed the presence at room temperature of DPPC-enriched gel domains up to several μm in size which protrude by 1.0 ± 0.1 nm from the smooth DOPC matrix (Fig. 1A). Following 150 min incubation with 50 μM hCT (9-32), a concentration used for peptide/cargo internalization by cells culture, the most striking topography change at low magnification concerned the DOPC matrix aspect which became grainy (Fig. 1B). No detectable change in the roughness and in the size of gel phase DPPC domains could be observed.

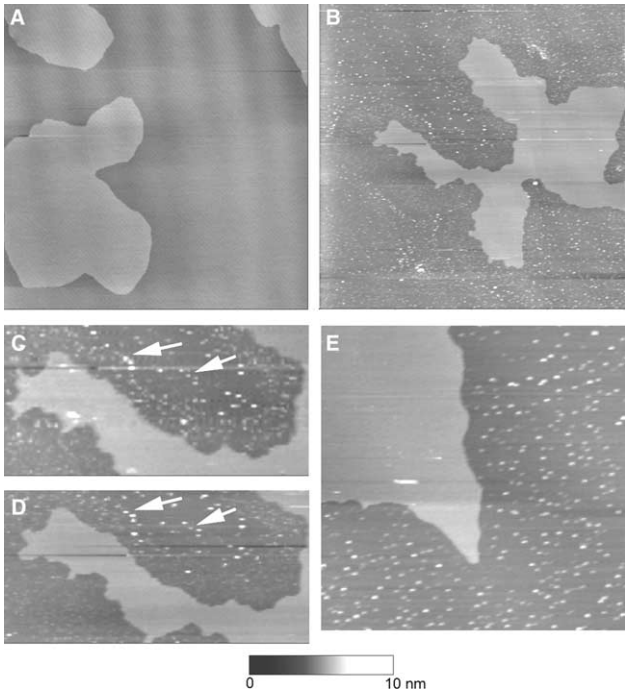

Fig. 1. Formation of hCT (9-32) aggregates in the DOPC enriched fluid phase. Upon addition of hCT (9-32) to DOPC/DPPC (1:1) supported bilayers (A), the darker fluid phase is covered with brigth dots (B). Peptide aggregates resist to successive scans of the same zone (C, D, arrows). Higher magnification reveals the globular shape of aggregates (E). AFM height images in buffer. Scan size: 10 μm (A, B), 5 μm (C, D), 2.5 μm (E).

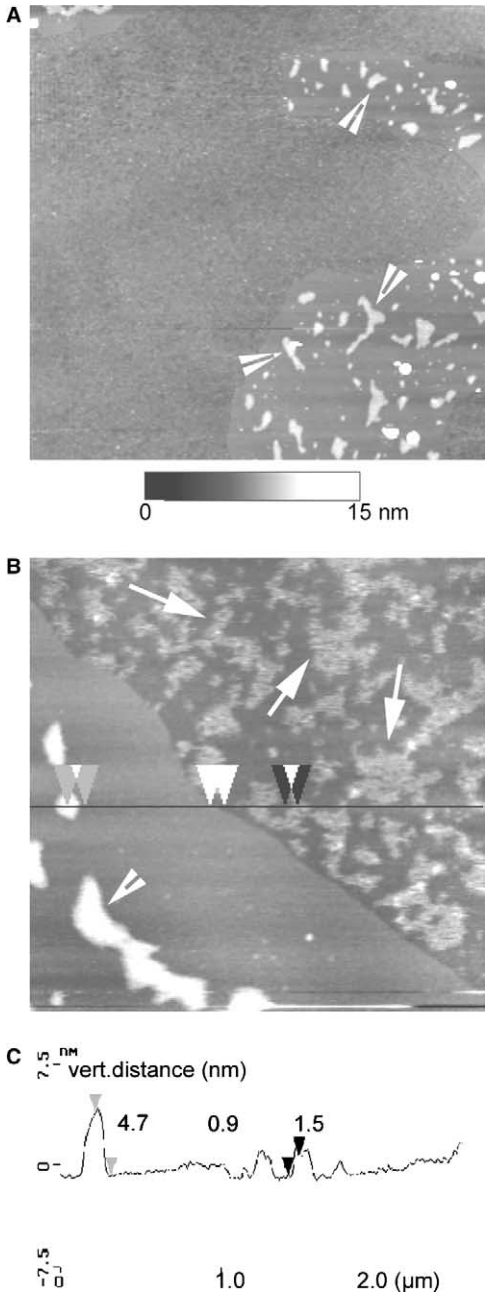

Fig. 2. Flat domain-like structures (arrows) decorate the bilayer fluid phase upon long duration incubation with hCT (9-32) (A, B). Peptide aggregates (arrow heads) are also visualized at the surface of gel domains. C is a virtual section of B. Scan size: 10 μm (A) and 2.5 μm (B).

Examination of samples at a higher magnification (Fig. 1C) revealed that the grainy aspect of the fluid phase was due to the presence of numerous globular aggregates, practically exclusively localized in the DOPC matrix, with no globular structures accumulated on the gel phase or at the fluid-gel interface. Except for a few large (300–500 nm) and tall (up to 15 nm) patches, the globular structures consisted of aggregates 76 ± 10 nm in diameter protruding from the matrix with ~1.5 nm maximum height. Aggregates were still present upon successive scans of the same zone (Figs. 1C and D, arrows) which indicates their anchoring resisted to the friction forces associated with scanning. Under identical incubation conditions, no

aggregates could be detected at the surface of bare mica (data not shown). Increasing the incubation time up to 16–18 h, the fluid phase matrix was markedly modified, and more difficult to discern from the gel phase at low magnification (Fig. 2): hCT (9-32) aggregates assembled to form domains-like structure, up to 300 nm in length, protruding by 1–2 nm above the DOPC fluid phase (Fig. 2B, arrows). For these long incubation periods, peptide aggregates of comparable size and up to 5 nm in height (Fig. 2C) decorated the gel phase domains (arrowheads). Brighter spots likely corresponding to surface contaminants were often observed following long duration incubations.

3.2. hCT (9-32)/eGFP cargo complexes localize in the DOPC/DPPC bilayer fluid phase

Contrasting with the results obtained for the peptide alone, incubation of hCT (9-32)/eGFP complex resulted in a significant and random adsorption of aggregates 50–90 nm in diameter at the surface of bare mica (Fig. 3A). Adding the complex to the DOPC/DPPC supported bilayers for 150 min induced a large modification of the fluid phase, leaving the gel phase unchanged (Fig. 3B). As compared to images obtained at identical magnification when incubating with the peptide alone, the fluid phase was characterized by the presence of many microdomain-like patches in addition to the small globular structures (Fig. 3C arrowheads). Reducing the scan size showed that microdomains-like patches consisted of clustered globular aggregates (62 ± 10 nm in diameter) which protruded ~4 nm from the fluid phase (Fig. 3C, arrows). They were often surrounded by a boundary emerging ~0.6 nm from the DOPC enriched fluid phase. At low magnification, the most striking changes in the topography of the bilayer, following 16–18 h incubations, were the clustering of hCT (9-32)/eGFP complexes, essentially in DOPC enriched fluid phase (Fig. 3D, arrows), with a few clusters present either at the fluid-gel phase boundary or on the gel phase domains (Figs. 3D and E, large arrowheads). Zones of the fluid phase bilayer appeared destabilized, being made of small and rough irregular microdomains 20–50 nm in length (Fig. 3D, thin arrows) eventually pierced by holes 50–140 nm in diameter (thin arrowheads).

3.3. Effect of cholesterol on hCT (9-32) and hCT (9-32)/eGFP cargo distribution

By inducing the formation of a liquid-ordered (l_o) phase that separates from the fluid phase, Chl plays a determinant role in the formation of microdomains in the plasma membrane of mammalian cells [19]. Addition of Chl to the DOPC/DPPC mixture resulted in the branching of the DPPC–Chl enriched l_o ordered domains (Fig. 4A), as previously reported [20]. The presence of Chl was associated with an enhanced sensitivity of bilayers to the peptide imposing a reduction in the incubation

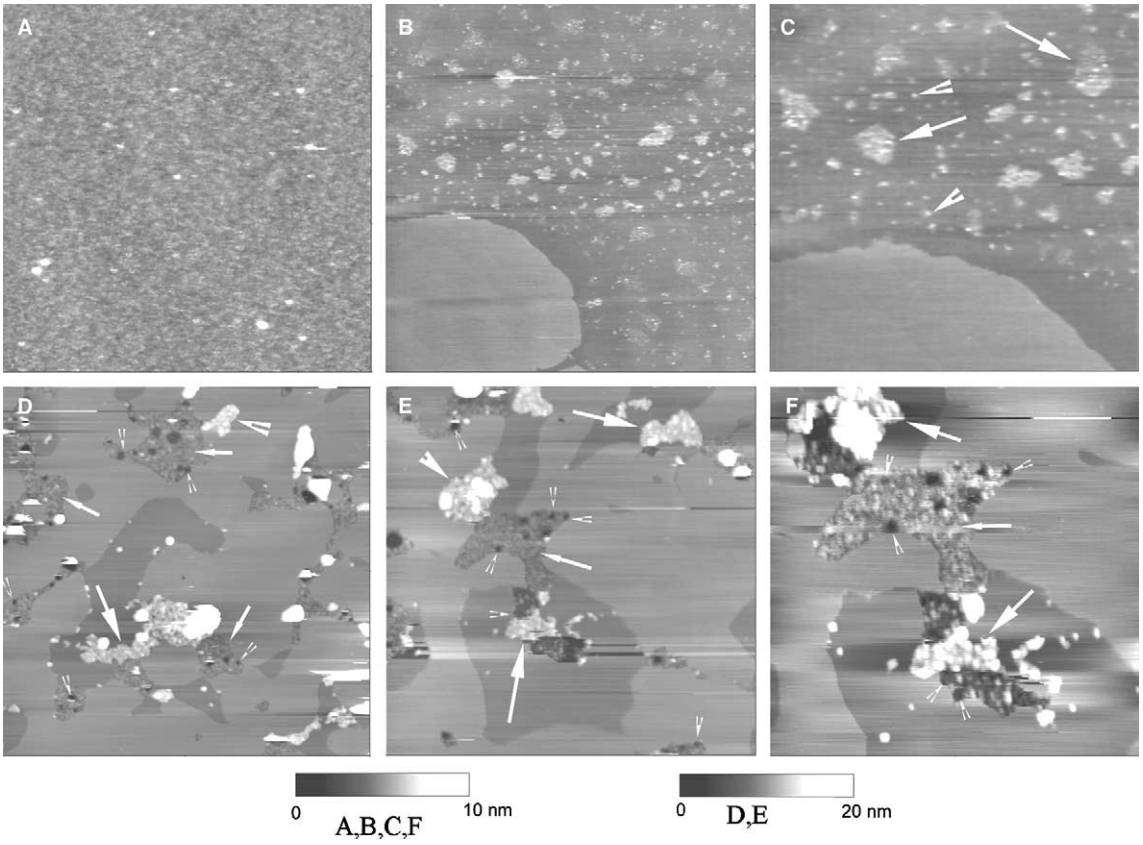

Fig. 3. hCT (9-32)/eGFP complex forms aggregates which adhere on mica surface (A, scan size 2.5 μm). After 2 h and 30 min incubation, aggregates (arrowheads) and clusters of aggregates organized into domains (arrows) are exclusively found in the bilayer fluid phase (B, C). Scan size: 10 μm (B), 5 μm (C). Domains of aggregates are still preferentially localized in the fluid phase (large arrows) but some are found at the phases boundary or on the gel phase (large arrow head) following long-time (16–18 h) exposure (D–F). By place, the fluid phase appears disorganised (thin arrows) and pierced by holes (thin arrow heads). Scan size: 5 μm (D), 3.4 μm (E), 2 μm (F).

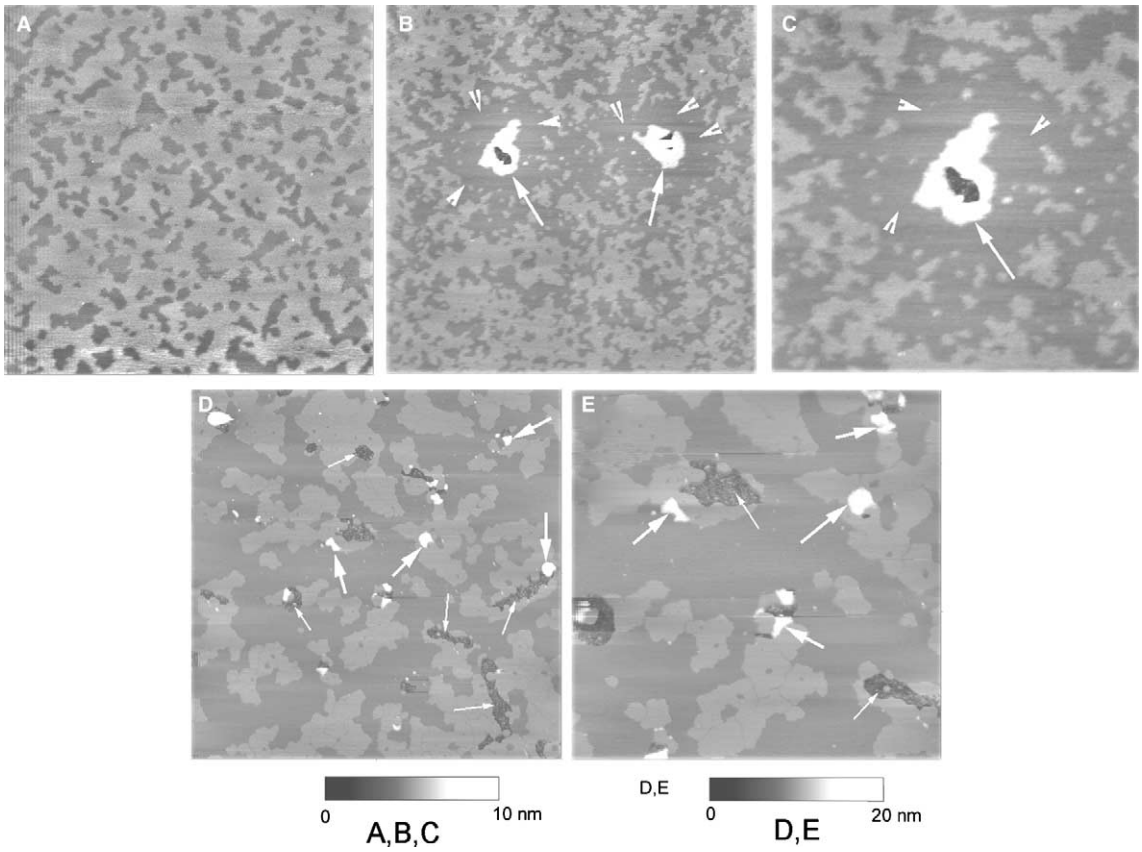

Fig. 4. Addition of Chl (DOPC/DPPC/Chl, 1:1:0.35) induces the formation of branched domains enriched in liquid-ordered lipids (A, scan size 5 μm). After 30 min incubation with hCT (9-32), the branched domains network is disorganized and disappears (arrowheads) in the vicinity of large aggregates of peptide (B, C, arrows). Scan size: 5 μm (B), 2.5 μm (C). Upon incubation with hCT (9-32)/eGFP complex for the same time, the bilayer topography is markedly modified (D, scan size 5 μm). Aggregates of hCT (9-32)/eGFP complexes are essentially found in the ordered phase domains (D, E, arrows) which are partly disrupted (thin arrows). Scan size (E): 2.5 μm.

time (30 min). With hCT (9-32) alone, aggregates assembled to form domains-like structure up to 600 nm in size generally pierced by large holes that perforate the bilayer (Figs. 4B and C, arrows). The aggregates were surrounded by a zone poor in l_o enriched domains (Figs. 4B and C, arrowheads) which strongly suggested the peptide had primarily interacted with and disrupted the branched domains. This view was supported by the perturbed organization of the branched network at a longer distance. In accordance with Chl-free samples, incubation with hCT (9-32)/eGFP complexes had a more marked effect on the bilayer topography. Branched domains were replaced by larger disconnected domains (Figs. 4D and E). Aggregates of hCT (9-32)/eGFP complexes were found practically exclusively on the l_o-enriched domains (arrows) where large holes were also frequently observed (thin arrows).

4. Discussion

4.1. hCT (9-32) forms aggregates whose localization depends on lipid composition

The data show that, under concentrations conditions required for the carrier peptide efficiency in cells, hCT (9-32) preferentially anchors either in the fluid or in the liquid-ordered phase of phase separated supported phosphatidylcholine bilayer, according to the presence of Chl. It is worth noting that with hCT (9-32) concentration 10 times lower, no modification of the bilayer topography could be noticed (data not shown). These data are in agreement with those obtained for salmon calcitonin where the peptide interacts with zwitterionic phospholipids only at high concentrations [21]. The C-terminal part of hCT plays an essential role in its carrier properties most likely via a conformational change in the presence of phospholipids, which could also induce the peptide self-assembly and interaction with the hydrophobic part of membranes [10]. The present observation of hCT (9-32) aggregates at the bilayers surface, whose size significantly increased as a function of time in DOPC/DPPC samples, strongly supports this hypothesis.

In absence of Chl, peptide aggregates were exclusively found in the bilayer fluid phase and no peptide accumulation at domain boundaries occurred, excepted for long-time exposures. On the other hand, the data suggested a preferential interaction of hCT (9-32) with the liquid-ordered phase in Chl containing bilayers. Such a redistribution was unexpected as regards to the literature which reports on preferential localization of transmembrane-α helical peptides [22,23] and amphipathic helical membrane active peptides [24] in the fluid phase of bilayers, even in the presence of Chl. A possible explanation to this behavior, which could also account for the associated marked increase in the sensitivity of membranes to the peptide deleterious effect, is that the presence of Chl in

ordered domains favored hCT (9-32) to adopt a different structure. Such a situation is found for amphipathic antimicrobial peptides which adopt α-helical, β-sheet, or both α-helical and β-sheet structures [25], with a structure-dependent lytic effect [26].

4.2. Peptide-dependent localization of hCT(9-32)/eGFP complexes in bilayers

Imaging of hCT (9-32)/eGFP complexes in buffer revealed the presence of aggregates distributed at random at the surface of bare mica. As compared to hCT (9-32) alone, this indicated a significant increase in the hydrophilic interaction between mica and complexes, which can be explained by the presence of the protein. Conversely, existence of aggregates in buffer should result from hydrophobic-driven self assembly of the peptide part of complexes. As for the peptide alone, hCT (9-32)/eGFP aggregates were localized exclusively in the fluid phase of the DOPC/DPPC bilayers, on the shorter incubation times, and in the ordered phase of DOPC/DPPC/Chl bilayers. This demonstrates that hCT (9-32) is capable to address the complex to specific regions of a bilayer. Incubation with hCT (9-32)/eGFP favored the formation of the microdomains-like patches. Although AFM does not allow to establish the local composition of these patches, i.e., peptide–peptide vs lipid–peptide, their size up to a few hundred nm suggests they can contain at least hundreds of peptide molecules (the molecular area of hCT (9-32) is close to 5 nm^2, unpublished data). This topography of peptide-treated bilayers suggests that hCT (9-32) CPP function may involve the carpet-like/toroidal pore mechanism proposed for antimicrobial peptides [8,9,25]. In this mechanism, peptides insert in the polar headgroups region thus creating a membrane thinning which finally induces transient defects or pores formation (see Fig. 3 in [25] for an illustration of the model). Moreover, peptide aggregation plays a major role in the formation of membrane defects [25]. Membrane destabilization, associated with the presence of holes in the bilayer perturbed regions, supports this hypothesis.

4.3. Concluding remarks

The modifications in the bilayer organization by hCT (9-32) and hCT (9-32)/eGFP were obtained using concentrations needed for their transport across cell membranes. This suggests that peptide aggregates-plasma membrane lipid interactions are involved in the carrier function of the peptide. Both the localization of the peptide–cargo complex, driven by the peptide part, and the time course of the interaction depend on the membrane lipid composition which might contribute to the selective activity of hCT (9-32) towards different cells.

Acknowledgements: This work was supported by the EU Grant QLK2-2001-01451.

References

[1] Derossi, D., Chassaing, G. and Prochiantz, A. (1998) Trends Cell Biol. 8, 84–87.
[2] Pooga, M., Hallbrink, M., Zorko, M. and Langel, U. (1998) FASEB J. 12, 67–77.
[3] Tung, C.H.T. and Weisslerder, M.D. (2003) Adv. Drug Deliv. Rev. 55, 281–294.
[4] Derossi, D., Calvet, S., Trembleau, A., Brunissen, A., Chassaing, G. and Prochiantz, A. (1996) J. Biol. Chem. 271, 18188–18193.
[5] Lindgren, M., Hällbrink, M., Prochiantz, A. and Langel, U. (2000) TIPS 21, 99–103.
[6] Richard, J.P., Melikov, K., Vives, E., Ramos, C., Verbeure, B., Gait, M.J., Chernomordik, L.V. and Lebleu, B. (2003) J. Biol. Chem. 278, 585–590.
[7] Epand, R.M., Shai, Y., Segrest, J.P. and Anantharamaiah, G.M. (1995) Biopolymers 37, 319–338.
[8] Pouny, Y. and Shai, Y. (1992) Biochemistry 31, 9482–9490.
[9] Yang, L., Harroun, T.A., Weiss, T.M., Ding, L. and Huang, H.W. (2001) Biophys. J. 81, 1475–1485.
[10] Schmidt, M.C., Rothen-Rutishauser, B., Rist, B., Beck-Sickinger, A.G., Wunderli-Allenspach, H., Rubas, W., Sadée, W. and Merkle, H.P. (1998) Biochemistry 37, 16582–16590.
[11] Tréhin, R., Krauss, U., Muff, R., Meinecke, M., Beck-Sickinger, A.G. and Merkle, H.P. (2004) Pharm. Res. 21, 33–42.
[12] Machova, Z., Muhle, C., Krauss, U., Tréhin, R., Koch, A., Merkle, H.P. and Beck-Sickinger, A.G. (2002) Chem. Biochem. 3, 672–677.
[13] Stipani, V., Gallucci, E., Micelli, S., Picciarelli, V. and Benz, R. (2001) Biophys. J. 81, 3332–3338.
[14] Mou, J., Czajkowsky, D.M. and Shao, Z. (1996) Biochemistry 35, 3222–3226.
[15] Vié, V., Van Mau, N., Chaloin, L., Lesniewska, E., Le Grimellec, C. and Heitz, F. (2000) Biophys. J. 78, 846–856.
[16] Rinia, H.A., Kik, R.A., Demel, R.A., Snel, M.M.E., Killian, J.A., van der Eerden, J.P.J.M. and de Kruijff, B. (2000) Biochemistry 39, 5852–5858.
[17] Dawson, P.E., Muir, T.W., Clark-Lewis, I. and Kent, S.B. (1994) Science 266, 776–779.
[18] Giocondi, M.C., Vié, V., Lesniewska, E., Milhiet, P.E., Zinke-Allmang, M. and Le Grimellec, C. (2001) Langmuir 17, 1653–1659.
[19] Simons, K. and Ikonen, E. (1997) Nature 387, 569–572.
[20] Milhiet, P.E., Giocondi, M.-C., Baghdadi, O., Ronzon, F., Roux, B. and Le Grimellec, C. (2002) EMBO Rep. 3, 485–490.
[21] Epand, R.M., Epand, R.F., Orlowski, R.C., Flanigan, E. and Stahl, G.L. (1985) Biophys. Chem. 23, 39–48.
[22] van Duyl, B.Y., Rijkers, D.T.S., de Kruijff, B. and Killian, J.A. (2002) FEBS Lett. 523, 79–84.
[23] Fastenberg, M.E., Shogomori, H., Xu, X., Brown, D.A. and London, E. (2003) Biochemistry 42, 12376–12390.
[24] Polozov, I.V., Polozova, A.I., Molotkovsky, J.G. and Epand, R.M. (1997) Biochim. Biophys. Acta 1328, 125–139.
[25] Shai, Y. (2002) Biopolymers 66, 236–248.
[26] Epand, R.F., Lehrer, R.I., Waring, A., Wang, W., Maget-Dana, R., Lelievre, D. and Epand, R.M. (2003) Biopolymers 71, 2–16.